Excitatory and inhibitory coupling in a one-dimensional array of Belousov-Zhabotinsky micro-oscillators: Theory

Vladimir K. Vanag and Irving R. Epstein

Phys. Rev. E **84**, 066209 — Published 27 December 2011

DOI: 10.1103/PhysRevE.84.066209

Excitatory and inhibitory coupling in a one-dimensional array of Belousov-Zhabotinsky micro-oscillators. Theory

Vladimir K. Vanag and Irving R. Epstein

Department of Chemistry, Brandeis University, Waltham, MA 02454-9110

Key words: spatiotemporal patterns, excitatory-inhibitory coupling, BZ micro-oscillators, coupled oscillators

We study numerically the behavior of one-dimensional arrays of aqueous droplets containing the oscillatory Belousov-Zhabotinsky reaction. Droplets are separated by an oil phase that allows coupling between neighboring droplets via two species: an inhibitor, Br_2, and an activator, $HBrO_2$. Excitatory coupling alone (through the activator) generates in-phase oscillations and/or "waves", while inhibitory coupling alone (through Br_2) gives rise to anti-phase oscillations, Turing patterns, and their combinations. The simultaneous presence of excitatory and inhibitory coupling leads to a large number of new spatio-temporal patterns, including some that exhibit very complex behavior. Analysis of a simple model allows us to simulate patterns resembling those observed experimentally under similar conditions and to elucidate the contributions of droplet and gap sizes, activator and inhibitor partition coefficients, and malonic acid concentration to the coupling strengths.

1. **Introduction**.

The study of coupled oscillators is one of the most important subfields of nonlinear science [1-6]. Synchronization, for example, arises from the coupling of oscillators in physics (e.g., Huygens's clocks [7]), chemistry [1], and biology (e.g., in coupled neurons [8]). Such phenomena as quorum sensing [9,10] result primarily from excitatory, i.e., attractive, coupling between oscillators, while multistability and multirhythmicity are due to inhibitory, or repulsive, coupling [11,12].

Recently, we developed a new experimental system for studying coupled chemical oscillators with local inhibitory coupling, consisting of an array of small (≅ 100 μm in diameter) identical water droplets separated by a surfactant monolayer from an oil phase and/or from each other. In the latter case, two monolayers of touching droplets can produce a bilayer [13,14]. Each droplet contains the reactants of the oscillatory Belousov-Zhabotinsky (BZ) reaction [15,16]: malonic acid (MA), bromate, sulfuric acid, ferroin (catalyst), and a small amount of $Ru(bpy)_3^{2+}$, which serves both as a cocatalyst and to make the BZ reaction photosensitive. Droplets are diffusively coupled through species dissolved in the oil phase, mainly Br_2, the inhibitor.

In that system, employing both one-dimensional (1D) [13] and two-dimensional (2D) [17] geometries, we observed a number of spatiotemporal patterns consisting of both oscillatory and stationary droplets. In 1D, we found Turing-like patterns, with mixtures of droplets in oxidized and reduced steady states, as well as anti-phase synchronization of oscillating drops. In a "1.5D" geometry consisting of two closely packed arrays of droplets in a capillary with a diameter between one and two times the droplet diameter, or in a hexagonal 2D geometry, we observed more complex patterns. In 1.5D, for example, we found one row of stationary droplets

and a second row of droplets oscillating anti-phase. The 2D phenomena include "π-S" patterns, in which in each triangle of adjacent droplets one is stationary and the other two oscillate antiphase, and "2π/3" patterns, in which the three droplets of a triangle oscillate 2π/3 out of phase with one another [17]. We were also able to generate in-phase synchronization (analogous to quorum sensing [10]) in 1D by initially synchronizing all droplets in our photosensitive system with a pulse of illumination. However, this regime is only metastable: after some time, one droplet suddenly undergoes a phase shift, which propagates through the system, eventually leading to the anti-phase regime. Such behavior is characteristic of strong inhibitory coupling.

In further experiments [18], we have discovered new synchronous regimes in a 1D array of coupled BZ droplets, in which two or three adjacent droplets oscillate in-phase, while neighboring doublets or triplets oscillate anti-phase with respect to one another. These experiments involve (*i*) a perfluorinated oil (3-ethoxy-1,1,1,2,3,4,4,5,5,6,6,6-dodecafluoro-2-trifluoromethyl-hexane) that increases the solubility of uncharged polar molecules, like the activator $HBrO_2$, and decreases the solubility of hydrophobic molecules, like Br_2, (*ii*) smaller gaps, or even no gaps, between water droplets, with the likely formation of a bilayer membrane between droplets in the case of direct contact, and (*iii*) a lower initial concentration of MA. In-phase oscillations have also been observed in an analogous system, in which the BZ water droplets in the continuous oil phase (squalane with the lipid mono-olein as the surfactant), were in contact, forming a bilayer [14]. We suggest that the patterns found emerge due to a combination of inhibitory and excitatory coupling. Here, we present theoretical support for this hypothesis, focusing on the effects of droplet spacing, partition coefficient, and MA concentration on coupling strength and pattern formation.

In Section 2 we describe, with the aid of partial differential equations (PDEs), a simple coupling between two water droplets separated by an oil gap as a reaction-diffusion problem. In Section 3, we depict the same situation by means of ordinary differential equations (ODEs) and compare the results with those obtained from the corresponding PDEs to obtain an appropriate form for the coupling term in the ODE treatment. In Section 4, we introduce our model for the BZ reaction and describe two BZ droplets coupled via activator and inhibitor with different coupling strengths. In Section 5, we extend our simulations to several (3 - 9) coupled in-line droplets. We conclude with a discussion in Section 6.

2. Coupling as a reaction-diffusion process (PDEs)

First, we simulate, using PDEs in 1D, the process of mass exchange between two water droplets, each of length a, separated by an oil gap of length b. In our simulations we use the software package FlexPDE [19], with a typical error (ERRLIM) of 4.0×10^{-7} for each variable in each spatial cell. In this section, we consider only one species, U. We vary the partition coefficient, P_U, of the diffusing molecule, labeled as U_1 or U_2 when it is present in water droplets 1 or 2, respectively, and as S in the oil gap. Thus $P_U = s_0/u_{10} = s_0/u_{20}$, where the subscript 0 designates equilibrium concentrations, and $u_1 = \int_0^a [U_1]d\xi / a$, $u_2 = \int_{a+b}^{2a+b} [U_2]d\xi / a$, and $s = \int_a^{a+b} [S]d\xi / b$, where ξ is the spatial coordinate with origin at the left end of droplet 1 (the oil gap and droplet 2 are to the right). To mimic the coupling between BZ droplets during the period of fast autocatalytic increase of activator followed by its fast decrease, we apply a short ($\Delta t = 0.2$ s) pulse to droplet 1 that increases the concentration u_1 from u_{10} to a maximum ($u_{1\_max} = 10^{-4}$), allow the system to evolve for a time t_p (usually larger than Δt, $t_p \cong 2$ s, similar to the duration of

the $HBrO_2$ pulse in the BZ reaction), and then apply to droplet 1 a negative pulse of the same magnitude and duration as the initial positive pulse (see Fig. 1c). Details of the PDEs, boundary conditions, and the procedure are given in Appendix 1 and in ref. [20]. At the end of the negative pulse, we measure the concentration of U_2, u_{2p}, and calculate the response, $R = 2(u_{2p} - u_{20})/u_{1\_max}$. If the coupling is very strong, the response is equal to unity, while for very weak coupling R is close to zero. The quantity R reflects the largest concentration of species U (above the equilibrium level u_{20}) that temporarily emerges in droplet 2 due to mass transport from droplet 1 under the condition that the pulse period t_p is comparable to or longer than the diffusion times, $a^2/(2D)$ or $b^2/(2D)$. If a and b are too small and $a^2/(2D) << t_p$ and $b^2/(2D) << t_p$, the coupling is obviously strong, but R is close to 0, since droplets 1 and 2 are almost in equilibrium. Another criterion for "strong" coupling may be chosen, though in this case the two regions are so close to each other that they should not be considered to be separate from a dynamical point of view.

In Fig. 1b, we observe a roughly inverse parabolic dependence of R on $\ln(P_U)$, i.e., R approaches zero at both high and low values of P_U and reaches a maximum in the neighborhood of $P_U = 0.1$ - 1 (the maximum depends on a and b). Intuitively, the response R is proportional to the rate of transfer of U from droplet 1 to droplet 2 and to the amount of U transferred. The rate of transfer is proportional to the diffusion characteristics (like a^2/D and b^2/D), while the amount transferred depends on the partition coefficient, P_U. The amount of U transferred from droplet 1 to the gap is small if P_U is small, and the amount of U transferred from the gap to droplet 2 (the reverse process) is small when the partition coefficient is large. Fig. 1b shows that if P_U is small (e.g., 0.001 or 0.01, as expected for polar molecules) then the response R, which is correlated with the coupling strength, is also small. The opposite is also true: if P_U is too large, the response R is

small. In some sense, the dependence of R on P_U is similar to the function $(x+1/x)^{-1}$, which has a maximum at $x = 1$.

Figure 1a demonstrates that if we decrease the gap (the length, b, or the diffusion time, $t_d = b^2/D_S$), the response increases. Comparing curves 1 and 2 in Fig. 1a, we see that the maximum value of R is almost the same for large and small P_U ($P_U = 1$ for curve 1 and $P_U = 0.01$ for curve 2). A decrease in the droplet length a (curve 3) leads to an increase in R (compare curves 2 and 3 in Fig. 1a, as well as curves 1 and 2 in Fig. 1b) due to faster transport of U molecules from distant portions of the droplet to the water/oil boundary, while a decrease in D_S (curve 4) results in smaller R because of slower diffusion through the gap. Thus, this set of computer experiments suggests that, even for rather small values of P_U, the coupling between water droplets can be effective if the oil gap is small enough.

3. Coupling described by ODEs

To test the roles of inhibitory and excitatory coupling, we should examine BZ droplets, i.e., an appropriate mathematical model of the BZ reaction. However even relatively simple BZ models, like the Oregonator [21], require significant computational time if they are employed in PDEs for systems of many coupled droplets. It is considerably easier to work with ODEs. To do this, we need to express the mass exchange process described above by PDEs in terms of ODEs. Although such a replacement of PDEs by ODEs can never be done exactly, as we have shown elsewhere [20], an adequate set of ODEs for this case is

$$du_1/dt = k_f r_V P_U (s_{12}/P_U - u_1)/(1 + r_V P_U) \quad (1)$$

$$ds_{12}/dt = k_f r_V^2 P_U (u_1 + u_2 - 2s_{12}/P_U)/(1 + r_V P_U) \quad (2)$$

$$du_2/dt = k_f r_V P_U (s_{12}/P_U - u_2)/(1 + r_V P_U) \quad (3)$$

where we introduce the subindex 12 for molecules in the oil gap between droplets 1 and 2. In one spatial dimension, r_V and k_f are given by

$$r_V = a/b; \;\; k_f \cong 2D/a^2 \tag{4}$$

i.e., r_V is the volume ratio between a water droplet and an oil gap for a 1D configuration, where a is the size of a water droplet. The physical meaning of k_f is that k_f^{-1} is the mean time for a species with diffusion coefficient D to diffuse across the distance a. The expression

$$C_U \equiv k_f r_V P_U/(1 + r_V P_U) \tag{5}$$

in eqs. (1)-(3) can be called the coupling strength. If $r_V P_U >> 1$, then C_U tends to k_f and is independent of r_V or P_U. Note that conservation of mass follows from (1)-(3)

$$u_1 + s_{12}/r_V + u_2 = constant \tag{6}$$

To examine how well eqs. (1)-(3) capture the behavior of the system, we consider Fig. 1d, as well as curve 5 in Fig. 1a and curve 3 in Fig. 1b, obtained from integration of ODEs (1)-(3). Comparing Figs. 1c and 1d, we see that the ODE kinetics is very similar to the PDE kinetics. This similarity holds for other parameters a, b, P_U, and D. Curves 3 and 4 in Fig. 1b are obtained at the same value of r_V and are quite close to one another. The coincidence of curves 2 and 5 (obtained at the same P_U) in Fig. 1a is less good, but still reasonable. We therefore have confidence that we can describe the mass exchange process by the ODEs (1)-(3).

4. Two coupled BZ droplets

4.1 Model

A mathematical model designed to describe the BZ reaction in water droplets should include Br_2, the inhibitor that diffuses through the oil gap, in addition to the three variables used

in the Oregonator. Previously, we developed such a four-variable model that was capable of describing complex phenomena including jumping waves [22].

$$dx/dt = - k_1xy + k_2y - 2k_3x^2 + k_4x(c_0 - z)/(c_0 - z + c_{min}) \quad (7)$$

$$dy/dt = -3k_1xy - 2k_2y - k_3x^2 + k_7u + k_9z + P(I) \quad (8)$$

$$dz/dt = 2k_4x(c_0 - z)/(c_0 - z + c_{min}) - k_9z - k_{10}z + P(I) \quad (9)$$

$$du/dt = 2k_1xy + k_2y + k_3x^2 - k_7u \quad (10)$$

where x, y, z, and u are the concentrations of activator ($HBrO_2$), inhibitor (Br^-), oxidized form of the catalyst (ferriin), and Br_2 (in water droplets), respectively; c_0 is the total concentration of catalyst (ferroin + ferriin); $P(I) = k(I)(c_0 - z)/(b_C/b + 1)$ is a term directly proportional to the intensity of illumination, $k(I)$, which can be introduced to characterize experiments with light perturbation; and k_i are rate constants: $k_1 = k_1'h$, $k_1' = 2 \times 10^6$ $M^{-2}s^{-1}$, $k_2 = k_2'h^2A$, $k_2' = 2$ $M^{-3}s^{-1}$, $k_3 = 3000$ $M^{-1}s^{-1}$, $k_4 = k_4'hA$, $k_4' = 42$ $M^{-2}s^{-1}$, $k_7 = k_7'$[MA], $k_7' = 29$ $M^{-1}s^{-1}$, $k_9 = k_9'$[MA], $k_{10} = k_{10}'$[MA], $k_{10}' = 0.05$ $M^{-1}s^{-1}$; $c_{min} = [2k_r(k_9 + k_{10})c_0]^{0.5}/k_{red}$, $k_r = 2 \times 10^8$ $M^{-1}s^{-1}$, $k_{red} = 5 \times 10^6$ $M^{-1}s^{-1}$. In general, the constant k_9' depends on the concentration of BrMA (bromomalonic acid), which in turn depends on [MA], [Br_2] and the time since mixing the reagents, since the production of BrMA is a slow process. The concentrations of MA, Br_2, and BrMA in water droplets depend in turn on partition coefficients of these species between water and oil. To simplify the situation, we choose $k_9' = 0.07$ $M^{-1}s^{-1}$ (in a few simulations we used $k_9' = 0.12$ $M^{-1}s^{-1}$), which gives the best fit between the experimental and theoretical z-profiles. In most of our simulations, $h = [H^+] = 0.15$ M and $A = [BrO_3^-] = 0.3$ M.

The ODEs in model (7)-(10) are quite stiff, with the characteristic time for autocatalysis around 1 s and the period of oscillations around 1000 s. In the numerical integration algorithm, the time step is automatically adjusted between about ca. 10^{-3} s and 10 s.

Model (7)-(10) was reduced from the Field-Körös-Noyes (FKN) model of the BZ reaction [23] and used by us previously in simulations of coupled BZ droplets [13]. The full FKN model contains the radical $BrO_2^{\bullet}$, which plays the role of activator and can diffuse in the oil gap, potentially leading to excitatory coupling. However, our simulations reveal that such coupling is very weak [13] and cannot lead to in-phase oscillations of neighboring droplets at a reasonable coupling strength. Therefore there is no need to use the more complex FKN model, and it suffices to use model (7)-(10), which contains the same primary activator, $HBrO_2$, as the FKN model.

Our hypothesis, which is supported by experimental results [18], is that the activator x is also able to diffuse in the oil gap or through the bilayer membrane, where we call it w. The partition coefficients for Br_2, P_U, and for $HBrO_2$, P_X, differ significantly. In separate experiments, we measured the partition coefficient P_U for the fluorinated oil and found that P_U = 2.5, while P_X is unknown but probably smaller than 0.1, since $HBrO_2$ (which quickly disproportionates via the reaction $2HBrO_2 \rightarrow BrO_3^- + HOBr + H^+$) is a polar molecule and poorly soluble in the hydrophobic oil. We next seek to understand why the experimentally found patterns, in which in-phase oscillating pairs or trios of BZ droplets oscillate anti-phase with one another, occur only at small [MA], which is incorporated into the rate constants k_7, k_9, and k_{10}. To answer this question, we analyze first a pair of coupled BZ droplets, i.e., a combination of eqs. (1)-(3) and (7)-(10), where eqs. (1)-(3) are applied to both variables u and x. For example, the final equations for the variable x are written as

$$dx_1/dt = - k_1x_1y_1 + k_2y_1 - 2k_3x_1^2 + k_4x_1(c_0 - z_1)/(c_0 - z_1 + c_{min}) + C_X(w_{12}/P_X - x_1) \quad (11)$$

$$dw_{12}/dt = r_V C_X(x_1 + x_2 - 2w_{12}/P_X) \quad (12)$$

$$dx_2/dt = - k_1x_2y_2 + k_2y_2 - 2k_3x_2^2 + k_4x_2(c_0 - z_2)/(c_0 - z_2 + c_{min}) + C_X(w_{12}/P_X - x_2) \quad (13)$$

where

$$C_X = k_f r_V P_X/(1 + r_V P_X) \quad (14)$$

Note that the coupling strengths C_X (excitatory) and C_U (inhibitory) are different, owing to the different partition coefficients, P_X and P_U (unless r_V is so large that $r_V P_X >> 1$). Note also that if r_V is very large, w_{12} rapidly reaches equilibrium, and, by setting $dw_{12}/dt = 0$ in eq. (12), we have $w_{12}/P_X = (x_1 + x_2)/2$. In this case, the coupling term in eqs. (11) and (13) assumes the familiar form $\pm C_X(x_1 - x_2)/2$, and the meaning of the coupling strength C_X is more evident.

4.2 Results

Simulating our system of two coupled BZ oscillators at different parameters k_f, r_V, P_X, and [MA], we find three different stable regimes (or modes), i.e., qualitatively different dynamical behaviors, (*i*) in-phase (IP) oscillations, (*ii*) anti-phase (AP) oscillations, and (*iii*) a so-called stationary Turing (T) mode, or inhomogeneous steady state (in the last case, the catalyst concentration , z, is close to its maximum, c_0, in one cell and is almost zero in the other cell). Such modes have been found in many other systems of two coupled identical oscillators [11,24,25]. There are two other dynamical modes of two coupled BZ oscillators at rather small r_V, when $a << b$: (*iv*) one oscillator exhibits large amplitude oscillations (with the amplitude of z close to c_0) and the other shows small amplitude oscillations (less than $0.01c_0$), i.e., almost suppressed oscillations; (*v*) a chaotic-like mode at still smaller r_V, in which both oscillators demonstrate alternating bursting with different numbers of spikes in each burst. We do not consider these modes further, since $a > b$ ($r_V > 1$) in our experiments. Note also that an "oscillator death" or "amplitude death" mode, in which both oscillators are in the same steady state [26], is theoretically possible, though we did not observe this mode in our simulations.

For two coupled BZ oscillators, the IP mode exists for any parameters, but it is stable to large-amplitude perturbations only in a limited region of the parameter space, which we designate as IP. We refer to the other regions as AP/IP or simply AP (where AP oscillations are stable, while IP is unstable to large-amplitude perturbation) and T/IP or simply T. Bistability between IP and AP oscillations (or between IP and T regimes) has been observed in other systems of two coupled oscillators [7,11,27]. We also find bistability between the T and AP regimes. The typical shape of AP oscillations is shown in Fig. 2a. Close to the AP/T transition, the AP oscillations assume the shape presented in Fig. 2b.

To examine the four-dimensional parameter space (k_f, r_V, P_X, and [MA]), we fixed two parameters and allowed the other two to vary. This variation can be performed in two different ways. In the first, a parameter is changed in small increments or decrements using the final state found with the previous parameter set as the initial state for the new parameters ("slow" variation). Alternatively, we can select values of our variables that correspond to a chosen mode, for example, AP oscillations, and use these initial conditions at a set of parameters that can be quite different from those at which this probe mode was obtained ("fast" variation). Note also that increasing k_f corresponds to decreasing a and proportionally lowering b, since r_V = *constant* [see eq. (4)]. Increasing P_X implies an increase in the coupling strength C_X only, which can be useful for analyzing the role of excitatory coupling. Increasing r_V corresponds to a decrease in b (since k_f and a are constants). Under the condition that $r_V > 1$ (and consequently $r_V P_U > 1$), an increase in r_V mainly leads to an increase in C_X (and only a slight increase in C_U) as well as a decrease in the average delay time between an "action" in cell 1 (2) and a "response" in cell 2 (1). In general, parameters r_V and k_f can be converted to parameters a and b [using eq. (4)] and the alternative parameter space (a, b, P_X, and [MA]) can be considered.

Results of our simulations are shown in Figures 3-7. In cases of the k_f-P_X, k_f–[MA], and [MA] - P_X parameter planes with "slow" variation of parameters, the three regions (or domains), IP, T, and AP, merge at a triple-point, a point where curves 1, 2, and 3 intersect. For example, in Fig. 3a, the AP-domain is situated to the left of curves 1 and 3, the IP-domain is above curves 1 and 2, while the T-domain is below curve 2 and to the right of curve 3. The T-domain is subdivided into three regions which we explain later. The position of the triple-point is strongly dependent on the other parameters, for example, on k_f, as shown in Figs. 3a and 2b, Fig. 5a and 5b, and Fig. 7. If the system switches to IP oscillations, then it remains there through any further small change of parameters (however if an asymmetric perturbation is large enough, the system can switch to either AP or Turing mode depending on its position in the parameter space). Therefore the transitions from AP to IP and from T to IP are unidirectional and are marked by single -headed arrows in all figures. The AP/T transition is reversible and can occur with or without hysteresis (i.e., subcritical or supercritical). A supercritical AP/T transition (via a supercritical Hopf bifurcation of the inhomogeneous steady state) is found in the k_f– [MA] plane (Fig. 4a) and in the [MA] - P_X plane (Fig. 5b) and is marked by a bidirectional arrow.

If the AP/T transition is subcritical, a region emerges in which both AP oscillations and the T-mode coexist. This region is marked as "AP/T" and lies between curves 3, 4, and 6 in Figures 3a, 3b and 4a, as well as between curves 1 and 3 in Fig. 5a. Curve 6 (in Figs. 3a, 3b, and 4a) marks the transition from AP to T, while curve 4 marks the AP/IP transition.

In Fig. 3c and 3d, we show where the various transitions occur if one parameter changes slowly. These two figures help to understand the transitions shown in Fig. 3a. Analogously, Figures 4b and 4c help to understand better the peculiar transitions happened in the k_f-[MA] parametric plane (Fig. 4a). For example, if we start at [MA] = 1 M at $k_f = 2.3$ s^{-1} (Fig. 4b) and

decrease [MA], AP oscillations become unstable at [MA] ≅ 0.7 M. However, at smaller [MA], between 0.09 M and 0.15 M, AP oscillations are stable again. At still smaller [MA], below 0.09 M, the Turing mode emerges supercritically.

Curve 5 in Fig. 3a, 3b, and Fig. 4a shows the result of using a fixed set of initial conditions (here corresponding to AP oscillations) as a probe to explore the parameter planes ("fast" variation). If the final pair of parameters (for example, P_X and k_f in Fig. 3a) belongs to the AP/T domain, we obtain AP oscillations. If this pair lies inside the small T-domain (between and below curves 5 and 6), then we obtain the T mode. If the parameters are inside the T/IP domain (between curves 2, 4, and 5), then the final behavior is IP oscillations. Thus, curve 5 separates the regions where IP oscillation is more or less probable than the T mode. Between curves 5 and 6 (the small T-domain), IP oscillations are also possible, but are unstable to large-amplitude perturbations. Analogously, in the AP/T region, AP oscillations are more probable than the T mode. Note that all three types of dynamical behavior (including IP) are possible in the AP/T domain, depending on initial conditions.

In Fig. 6a, we examine the dependence of the boundary between the IP and AP (or AP/IP) domains in the r_V-P_X parametric plane as a function of [MA] (this line corresponds to curve 1 in Figs. 3a, 3b, 4a, and 5). The AP/IP region shrinks as [MA] decreases, which suggests that at small [MA] in-phase oscillations are more stable for a set of N BZ droplets, and, as a result, pairs of oscillating in-phase neighboring BZ drops can emerge. Curves 1 – 4 in Fig. 6a are well approximated as

$$P_X = constant/r_V \tag{15}$$

i.e., the product $r_V P_X$ determines the boundary between the IP and AP/IP domains. This product also determines the coupling strength C_X [see eq. (14)]. In general, the boundary between the IP

and AP/IP regions at constant [MA] and k_f depends on the ratio between the coupling strengths C_U and C_X; an increase in C_U favors AP oscillations, whereas an increase in C_X promotes IP oscillations (see Fig. 6b).

4.3 Analysis

In an effort to understand in greater depth why a decrease in [MA] broadens the IP region, we plot the ratios between the activator (x) and inhibitor (y and u) concentrations during the autocatalytic spike in the BZ reaction. In Figs. 6c and 6d, we see that these ratios depend strongly on [MA], and consequently the sensitivity of the system to inhibitory and excitatory coupling should also depend on [MA]. However, as is often the case in nonlinear systems, a simple interpretation without a detailed analysis is elusive. Such a detailed analysis was done recently for two coupled Huygens clocks oscillating in a harmonic regime [7], but we are unaware of similar analyses for a pair of coupled chemical relaxation oscillators.

Since the system behavior is most sensitive to parameter changes near the triple point,and since the region of tristability (domain AP/T) is very close to the triple point, it is important to determine the position of the triple points in the parameter space. Eqs. (14) and (15) suggest that changes in r_V can be compensated by varying P_X. Therefore we fix $r_V = 10$ and reduce the 4-dimensional parameter space to a 3-dimensional space: P_X, k_f, and [MA].

The trajectory of the triple point in the k_f-P_X-[MA] space is shown in Fig. 7a as two projections "P_x" and "MA" on the k_f-P_X and k_f-[MA] planes, respectively. Both lines "Px" and "MA" are well fitted by power dependences $P_X = C_1 k_f^{-0.65}$ and $[MA] = C_2 k_f^{0.56}$, respectively. To clarify how "Px" is obtained, we copy in Fig. 7b curves 1a and 1b which are the boundaries between the IP and AP domains in Figs. 3a and 3b, respectively. The bottom ends of these lines

are the triple points at [MA] = 0.03 M and 0.056 M. The dotted line connecting the ends of these lines is a portion of the line "Px" in Fig. 7a.

Finally, note that the period of IP oscillations is always shorter than the period of AP oscillations. This difference, which ranges from a few percent to a factor of two, depending on the coupling strength C_U, is one of the reasons for the very complex behavior we find when more than two identical BZ droplets are coupled.

5. Several (3 to 9) coupled BZ droplets

Now we seek to answer our main question, i.e., how the combination of excitatory and inhibitory coupling affects pattern formation in a 1D array of BZ droplets. Armed with our knowledge of how the boundaries between the IP, AP, and T regions depend on [MA] and the coupling strength (including parameters k_f, P_X, and r_V), we can now simulate 1D arrays of coupled BZ droplets similar to those studied experimentally [18] and theoretically [13]. We pay special attention to parameter regions where bi- or tristability between different dynamical modes occurs in the case of two coupled oscillators. However, comparison between modes found for two and N coupled oscillators should be done with caution.

5.1 Model equations

We consider here two different boundary conditions, fixed value and periodic (i.e., circularly coupled oscillators). If we use symmetrical fixed value boundary conditions and oil drops are placed at the ends of our linear array of droplets, then the oil drop at the left end is described by the following equations:

$$ds_L/dt = r_V k_f r_V P_U(u_L + u_1 - 2s_L/P_U)/(1 + r_V P_U) \quad (16)$$

$$dw_L/dt = r_V k_f r_V P_X (x_L + x_1 - 2w_L/P_X)/(1 + r_V P_X) \quad (17)$$

The subindex L refers to the leftmost oil droplet. Similar equations hold for the rightmost droplet with L replaced by R, 1 by N, and $u_L = u_R = u_T$, $x_L = x_R = x_T$. In this case, the two end droplets are not identical with the other N-2 droplets, since they interact with the constant concentrations of inhibitor, u_L, and activator, x_L. If our boundaries are instead impermeable walls, then $u_T = x_T = 0$. In some of our experiments, we observe two (or more) stationary droplets (either in oxidized or reduced states) between which there are several oscillatory droplets. To simulate the dynamics of a set of these oscillatory droplets, we can use fixed values u_T and x_T corresponding to the concentrations of u and x in the adjacent stationary droplets. Usually these adjacent stationary droplets are in the reduced state, and the concentrations of u_T and x_T can be taken from simulations of stationary Turing-like patterns. We use $u_T \cong 4 \times 10^{-6}$ M and $x_T = (6\text{-}7) \times 10^{-8}$ M for our chosen concentrations of $[H^+]$, $[BrO_3^-]$, and [MA].

For a 1D array of N water droplets with fixed-value boundary conditions, the equations are

$$dx_n/dt = - k_1 x_n y_n + k_2 y_n - 2k_3 x_n^2 + k_4 x_n (c_0 - z_n)/(c_0 - z_n + c_{min}) + k_f r_V P_X (w_{n-1,n}/P_X + w_{n,n+1}/P_X - 2x_n)/(1 + r_V P_X) \quad (18)$$

$$dy_n/dt = -3k_1 x_n y_n - 2k_2 y_n - k_3 x_n^2 + k_7 u_n + k_9 z_n \quad (19)$$

$$dz_n/dt = 2k_4 x_n (c_0 - z_n)/(c_0 - z_n + c_{min}) - k_9 z_n - k_{10} z_n \quad (20)$$

$$du_n/dt = 2k_1 x_n y_n + k_2 y_n + k_3 x_n^2 - k_7 u_n + k_f r_V P_U (s_{n-1,n}/P_U + s_{n,n+1}/P_U - 2u_n)/(1 + r_V P_U) \quad (21)$$

$$ds_{n,n+1}/dt = r_V k_f r_V P_U (u_n + u_{n+1} - 2s_{n,n+1}/P_U)/(1 + r_V P_U) \quad (22)$$

$$dw_{n,n+1}/dt = r_V k_f r_V P_X (x_n + x_{n+1} - 2w_{n,n+1}/P_X)/(1 + r_V P_X) \quad (23)$$

for $n = 1, 2, ..., N$, with $s_{0,1} \equiv s_L$, $w_{0,1} \equiv w_L$, $s_{N,N+1} \equiv s_R$, $w_{N,N+1} \equiv w_R$.

For periodic boundary conditions, u_L and x_L in eqs. (16) and (17) are replaced by u_N and x_N, respectively; s_L and w_L are renamed as $s_{1,N}$ and $w_{1,N}$, respectively, and the variables s_R and w_R are eliminated. In other words, droplets 1 and N are neighbors.

Each water droplet, except the two end droplets in the case of fixed value boundary conditions, has two neighboring water droplets, whereas in the case of two coupled oscillators, each droplet has only one neighbor. Therefore, the coupling strength for N linearly coupled droplets ($N > 2$) is effectively doubled (at the same k_f, P_X, and r_V) relative to the case of two coupled droplets.

In our previous simulations with the FKN model [13], we found several exotic modes for even numbers (4 or 6) of coupled oscillators, while these modes were not found for odd numbers of oscillators (5, for example). This means that at least some of these modes are "symmetry-sensitive". Therefore, we must examine arrays with both even and odd numbers of water droplets if we want to find modes that are "stable" with respect to the number of oscillators. This observation gives rise to a more general question: how many droplets are needed to represent a very large row of water droplets in a capillary? In our experiments we have several tens or even hundreds of BZ droplets separated by oil gaps. Can we simulate the behavior of such a large array of droplets using fewer than 10 droplets?

5.2 Results

We first present selected space-time plots obtained by numerical integration of eqs. (16)-(23) for a variety of parameters and initial conditions for periodic boundary conditions and arrays of three to nine water droplets. We investigate how the number of droplets, N, affects the observed patterns. To do this, we fix all parameters ([MA] = 0.02 M, $r_V = 10$, $k_f = 0.45$ s^{-1})

except P_X. For each array size N, we vary P_X and select different initial conditions to find as many different patterns as we can. Note that this method cannot guarantee finding all possible patterns, since the number of initial conditions is infinite, but we think that we have found all major patterns, since we investigated a wide range of initial conditions including anti-phase, in-phase, Turing-like patterns, and combinations of them, as well as more complex patterns obtained in the course of simulations. The results of these simulations are shown in Figs. 8 – 13.

In these numerical experiments, the parameters are chosen in such a way that the system exhibits Turing (T) patterns at small P_X (< 0.001) and in-phase (IP) oscillations at large P_X (> 0.01). If the parameter k_f (= 0.45 s^{-1} in these set of simulations) is decreased below 0.35 s^{-1}, AP emerges at small P_X instead of Turing patterns (an example of such AP patterns is shown in Fig. 11a). Therefore, we are close to the AP/T boundary at small P_X. In the range of P_X between 0.001 and 0.01, there are many different patterns, including anti-phase oscillatory clusters (APOC) and anti-phase oscillatory clusters with common droplet(s) (APOCwCD). For 3 droplets (Fig. 8b), we find APOC in which one cluster consists of two droplets, while the other consists of a single droplet. In the case of 4 droplets (Fig. 8f), both clusters consist of two droplets. In addition to APOC, two new patterns emerge: anti-phase oscillations (AP) (Fig. 8e) and APOCwCD (Fig. 8g). AP patterns exist only for even numbers of droplets (4, 6 and 8) and are unstable to large perturbations at our chosen parameters. APOCwCD patterns usually lie between APOC and IP patterns in the parameter space. In Fig. 8g, the two anti-phase oscillatory clusters consist of single droplets, numbers 2 and 4 (numbering from the left), while the common droplets, which oscillate with double frequency, are droplets 1 and 3.

With 5 and 6 droplets (Figs. 9 and 10), an additional pattern emerges (see Figs. 9b and 10d) that we call APOC(1:2)wSD (anti-phase oscillatory clusters with special droplet). The ratio

(1:2) signifies that the droplets in one cluster (droplets 3 and 5 in Fig. 9b) have one spike per period, while droplets in the other cluster (droplets 1 and 2 in Fig. 9b) exhibit two spikes. Oscillations of the special droplet (droplet 4 in Fig. 9b and droplet 1 in Fig. 10d) have a profile like the one in Fig. 2b. The patterns shown in Figs. 9d and 9e can be considered as intermediate between APOC and APOCwCD. The numbers of droplets in the clusters of the APOC patterns are 2 and 3 in Fig. 9c and 3 and 3 in Fig. 10c.

We do not find any new patterns with 7 droplets (Fig. 11). We see T-patterns, APOC(1:2)wSD, and APOC. In Fig. 11a, we show what happens to the AP patterns that emerge at small k_f in the case of odd numbers of droplets: two droplets start oscillating in-phase, destroying the very symmetric AP patterns (like those in Figs. 10b or 12b)

Increasing the number of droplets to 8 (Fig. 12), we observe another new pattern that can be called "moving defects" (Figs. 12c and 12d). The defect is a phase shift between oscillatory clusters, but the constitution of these clusters is not stationary in time. A cluster can lose one or two droplets and acquire another one or two neighboring droplets, giving the appearance of moving defects. An analogous moving defect (which reflects from the ends of the droplet array) is observed for 6 coupled droplets with fixed-value boundary conditions at slightly different parameters (Fig. 12g). The APOCwCD pattern in Fig. 12f is similar to the pattern in Fig. 8g, except that the anti-phase oscillatory clusters now consist of three droplets (2-4 for one cluster and 6-8 for the other).

In the case of 9 droplets (Fig. 13), we again find new patterns, shown in Figs. 13b-d and 13f. The pattern in Fig. 13b is similar to APOC(1:2)wSD, but we now have three clusters, and we designate the pattern as APOC(1:2:2)wSD. The oscillations of the special droplet, 5, in Fig.

13c are also new, with alternating long and short spikes. The pattern in Fig. 13f resembles APOCwCD but with defects.

We conclude that an increase in the number of droplets leads in general to the emergence of qualitatively new patterns. It appears that a relatively small number of droplets cannot be representative of a long sequence of coupled droplets. However, some specific (and relatively simple) patterns in large arrays can be simulated with a small number of drops. The range of P_X at which generic patterns like T or APOC survive depends on the number, N, of droplets. For example, the P_X-ranges for APOC patterns are 0.0035-0.004 for $N = 3$, 0.001-0.005 for $N = 4$, 0.003-0.004 for $N = 5$, 0.002-0.007 for $N = 6$, and 0.003-0.007 for $N = 7$. Note also that different patterns can coexist at the same parameters, and this coexistence is also N-dependent.

In the above described set of computer experiments with periodic boundary conditions, we were able to reproduce APOCwCD patterns seen in our experiments, but with one discrepancy: our APOCwCD patterns are not surrounded by stationary (Turing) droplets, as they are in experiment. We now examine what happens if we use fixed-value boundary conditions. First, we show in Fig. 14 that different boundary conditions give rise to entirely different patterns: for periodic boundary conditions (Fig. 14a), we see anti-phase oscillations that look like cascade patterns (since the phase shift between neighboring droplets is not exactly $T/2$); combinations of stationary and anti-phase oscillatory droplets are shown in Fig. 14b ($u_T = 4 \times 10^{-6}$ M, $x_T = 6 \times 10^{-8}$ M); and Turing patterns are presented in Fig. 14c ($u_T = x_T = 0$).

In Fig. 15, we exhibit patterns found for $u_T = 4 \times 10^{-6}$ M and $x_T = 6 \times 10^{-8}$ M boundary conditions when we vary P_X. For this set of experiments, k_f was chosen in such a way ($k_f = 0.3$ s^{-1}) that our system tends to go to AP or cascade oscillations at small P_X. However, due to the boundary conditions, the two end droplets do not oscillate in Fig. 15a. An increase in P_X leads to

complex patterns (Fig. 15b and 15c) in which the number of neighboring droplets oscillating in-phase increases. At still larger P_X, APOC patterns (Fig. 15d), a mixture between APOC and APOCwCD patterns (Fig. 15e) emerge. Finally, at sufficiently large P_X, only IP patterns remain.

Next we consider what happens if we vary k_f (Fig.16 and 17) or [MA] (Fig. 18). In Fig. 16, we show patterns observed at small P_X and $u_T = x_T = 0$ for 6 droplets. At $k_f = 0.2$, we find 3 different patterns (Fig. 16a-c). Patterns in Figs. 16a and 16b are combinations of 4 stationary and 2 oscillatory droplets either anti-phase (Figs. 16a) or in-phase (Figs. 16b). These two patterns demonstrate that stationary droplets can coexist with oscillating droplets at fixed value boundary conditions. In Figs. 16c and 16d, we see complex patterns with very long global periods T_g equal to 5379 s and 8312 s, respectively, while the average period between two spikes is 672-768 s for Fig. 16c and 831-1039 s for Fig. 16d (different droplets have different average periods). At larger k_f (0.4-0.5 s^{-1}), we see different Turing patterns (Figs. 16e and 16f).

In Fig. 17, we show patterns observed at large P_X and $u_T = 4 \times 10^{-6}$ M, $x_T = 7 \times 10^{-8}$ M for $N = 5$. There are no stationary droplets at this set of parameters (except "droplets 0 and N+1" that constitute the fixed-value boundary conditions). At $k_f = 0.1$ (Fig. 17a), we see APOC patterns. The patterns in Figs. 17b and 17c are mixtures of APOC and APOCwCD patterns. At still larger k_f (Fig. 17d), we have the striking APOCwCD pattern, observed experimentally, in which the central droplet has double frequency, alternately flashing in-phase with its two neighbors to the left and right. At still larger k_f (Fig. 17e), the system goes to IP patterns.

Fig. 18, in which we vary [MA], is interesting because IP patterns are found both at small (0.02-0.025 M) and at large (0.2-0.8 M) concentrations of MA, while APOCwCD and similar patterns are found at moderate [MA]. Thus, if we start our experiment at relatively large [MA], we first see IP patterns , then as [MA] decreases we obtain anti-phase clusters of in-phase

oscillating neighboring droplets, but finally, at very small [MA], we return to IP patterns, now with a long period.

6. Discussion and Conclusion

By including both excitatory and inhibitory coupling in our simulations, we have found many new periodic regimes, both simple and complex, in a system of diffusively coupled chemical oscillators in 1D. These patterns, which are very similar to those found experimentally [18], occur at small distances between BZ droplets or even when BZ droplets are in contact, and at relatively small concentrations of malonic acid. Whereas inhibitory coupling is effective at both small and large gaps between BZ droplets (up to 300 μm [13]), excitatory coupling through the polar activator, $HBrO_2$, diffusing through the oil gap, is effective only for very small gaps and relatively high partition coefficient P_X (but still much smaller than P_U), which requires an oil with a relatively high dielectric constant like HFE-7500 [18].

Though our model assumes the presence of a hydrophobic oil gap between water droplets and different partition coefficients for the activator and inhibitor in this gap, it is easily extended to the case of a hydrophobic bilayer membrane between water droplets [14], simply by considering P_X as the partition coefficient between the bilayer and the aqueous phase, as well as by reducing b (the size of the gap) to a few nanometers (in Fig. 1a, the smallest value of $t_d/t_p = 10^{-6}$ corresponds to 60 nm). Note that transfer of a polar molecule from water to water through a narrow hydrophobic region is considered here as a simple classical passage over a potential barrier, where the particle has a larger energy than the barrier potential.

Our computer simulations reveal a large number of different regimes, presented as space-time plots, in a rather narrow region of coupling strengths, C_X (activator) and C_U (inhibitor). If

C_X increases at constant C_U, the system goes to the IP regime, while if C_X decreases, we see the AP regime or Turing patterns (depending on C_U). The contribution of k_f to the coupling strengths, C_X and C_U, appears to be critical for the emergence of Turing patterns. We note the prevalence of multistability, i.e., the existence of multiple stable patterns, depending on initial conditions, at the same set of parameters, particularly for larger droplet arrays. Note also that the spatially extended system corresponding to system (7)-(10), but with normalized diffusion coefficients $D_U = 1$, $D_X << 1$ (since $C_X << C_U$), and $D_Y = D_Z = 0$ (since molecules Y and Z cannot diffuse outside the water droplets) has Turing and Hopf or saddle instabilities (with two positive eigenvalues at wavelength $k = 0$). Interaction between Turing and Hopf or between Turing and saddle instabilities can lead to several phenomena, including in-phase and anti-phase oscillatory Turing patterns [28-31]. In a narrow region between in-phase and anti-phase oscillatory Turing patterns, chaotic-like behavior has been observed in computer simulations [28,29]. We suggest that something similar can occur in the present system of coupled BZ oscillators, i.e., in a narrow region of parameters C_X and C_U, between the in-phase and anti-phase regimes, chaotic-like behavior or a very complex periodic pattern with a very long global period becomes possible, and many different and less complex periodic regimes arise close to the chaotic-like regime. Note also that no chaotic-like behavior is observed for two coupled BZ droplets.

Our investigations show that we can control and change patterns by tuning the coupling strengths C_X and C_U, either by varying the distance between droplets or by modifying the partition coefficients of the activator and/or the inhibitor. Of course, it is difficult, perhaps impossible, to change the partition coefficients after the system is prepared. It may be possible, however, to control the coupling strengths by introducing into the gap species that can react

selectively with the activator or the inhibitor. The distance between droplets also can be controlled dynamically by using, for example, a gel [32] whose volume is sensitive to the redox potential of the catalyst, $Ru(bpy)_3$. Such experiments might lead to materials with interesting, and potentially useful, patterns of chemomechanical transduction. This notion might be tested by incorporating mechanical forces into the reaction-diffusion model used here [33].

Note also that different regimes (like IP, Turing or AP) of initially identical coupled cells lead to different consumption of initial reagents, like MA or BrO_3^-, by these cells, which in turn leads to deviations in the natural frequencies of the oscillatory droplets (if they are uncoupled). These dynamically induced variations in the individual cell dynamics may lead in turn to new dynamical patterns of the coupled oscillators. Small differences in droplet size, *a,* and in gap size, *b,* inherent in the experiments, result in a form of noise in the coupling strength between droplets, which may also lead to new dynamical regimes. We saw that fixed-value boundary conditions, which affect only the end droplets, resulted in new patterns (see, for example, Fig. 14). Therefore it seems likely that variations of *a* or *b* can also induce the emergence of new patterns.

Note also that our inhibitor is Br_2, not Br^-, which is usually considered to be the inhibitor in the BZ reaction. If we use Br^- as the inhibitor in our simulations (hypothetically, since Br^- cannot diffuse in the oil phase), we are not able to find Turing patterns, and anti-phase oscillations of two inhibitorily coupled BZ droplets occur only in a very narrow parametric region. A detailed consideration of the different inhibitory roles of Br_2 and Br^- is beyond the scope of this work.

Koseska et al. [34] recently analyzed a model system of 2-18 globally coupled (through a mean field concentration of signaling molecule) synthetic genetic oscillators (“repressilators”).

They also observed multiple attractors whose numbers increased with the number of oscillators, and they suggest that the formation of clusters in these patterns may provide a mechanism for dynamical differentiation in biological systems, with the size of the population playing "a crucial role in determining which dynamical behavior is likely to be dominant". It has also been suggested that an appropriate balance between inhibitory and excitatory synapses [8,35] is needed to maintain the brain in a regime that lies close to the chaotic one, since the information capacity of such a regime is maximal [36]. Perhaps the present system, since it can be easily tuned, may provide a useful analog amenable to detailed analysis.

Acknowledgements. This work was supported by the National Science Foundation through grants CHE-0526866 and MRSEC grant DMR-0820492 and by the Army Research Office through grant W91NF-09-0496. I.R.E. thanks the Radcliffe Institute for Advanced Study for a fellowship. We thank Jorge Delgado for discussions and Ivan Valent for measuring partition coefficients.

Reference List

[1] I. R. Epstein and J. A. Pojman, *An Introduction to Nonlinear Chemical Dynamics* (Oxford University Press, New York, 1998).

[2] A. Pikovsky, M. Rosenblum, and J. Kurths, *Synchronization. A universal concept in nonlinear sciences.* (University Press, Cambridge, 2001).

[3] S. H. Strogatz and I. Stewart, Scientific American **269,** 102 (1993).

[4] Y. Kuramoto, *Chemical Oscillations, Waves, and Turbulence* (Springer, Berlin, 1984).

[5] S. Boccaletti *et al.*, Phys. Rep. **366,** 1 (2002).

[6] V. S. Afraimovich, V. I. Nekorkin, G. V. Osipov, and V. D. Shalfeev, *Stability, structures and Chaos in nonlinear synchronization network* (World Scientific, 1995), Vol. v. 31.

[7] R. Dilão, Chaos **19,** 023118 (2009).

[8] E. M. Izhikevich, *Dynamical Systems in Neuroscience: The Geometry of Excitability and Bursting* (MIT Press, Cambridge, 2007).

[9] A. Camilli and B. L. Bassler, Science **311,** 1113 (2006).

[10] A. F. Taylor *et al.*, Science **323,** 614 (2009).

[11] M. N. Stolyarov, V. A. Romanov, and E. I. Volkov, Phys. Rev. E **54,** 163 (1996).

[12] E. I. Volkov and D. V. Volkov, Phys. Rev. E **65,** 046232 (2002).

[13] M. Toiya, V. K. Vanag, and I. R. Epstein, Angew. Chem. Int. Ed. **47,** 7753 (2008).

[14] S. Thutupalli, S. Herminghaus, and R. Seemann, Soft Matter **7,** 1312 (2011).

[15] B. P. Belousov, in *Collection of Short Papers on Radiation Medicine*, (Medgiz, Moscow, 1959), p. 145.

[16] A. M. Zhabotinsky, Proc. Acad. Sci. USSR **157,** 392 (1964).

[17] M. Toiya *et al.*, J. Phys. Chem. Lett. **1,** 1241 (2010).

[18] J. J. Delgado *et al.*, to be submitted (2011).

[19] FlexPDE, http://www.pdesolutions.com (2010).

[20] V. K. Vanag and I. R. Epstein, Phys. Rev. E **81,** 066213 (2010).

[21] R. J. Field and R. M. Noyes, J. Chem. Phys. **60,** 1877 (1974).

[22] V. K. Vanag and I. R. Epstein, J. Chem. Phys. **131,** 104512 (2009).

[23] R. J. Field, E. Körös, and R. M. Noyes, J. Am. Chem. Soc. **94,** 8649 (1972).

[24] I. Schreiber and M. Marek, Physica D **5,** 258 (1982).

[25] I. Schreiber, M. Holodniok, M. Kubicek, and M. Marek, J. Stat. Phys. **43,** 489 (1986).

[26] D. V. Ramana Reddy, A. Sen, and G. L. Johnston, Phys. Rev. Lett. **80,** 5109 (1998).

[27] V. K. Vanag and I. R. Epstein, J. Chem. Phys. **119,** 7297 (2003).

[28] J. Carballido-Landeira *et al.*, Phys. Chem. Chem. Phys. **10,** 1094 (2008).

[29] A. Kaminaga, V. K. Vanag, and I. R. Epstein, J. Chem. Phys. **122,** 174706 (2005).

[30] R. McIlwaine, V. K. Vanag, and I. R. Epstein, Phys. Chem. Chem. Phys. **11,** 1581 (2009).

[31] V. K. Vanag and I. R. Epstein, Phys. Rev. E **71,** 066212 (2005).

[32] R. Yoshida, H. Ichijo, T. Hakuta, and T. Yamaguchi, Macrom. Rapid Commun. **16,** 305 (1995).

[33] V. V. Yashin and A. C. Balazs, Science **314,** 798 (2006).

[34] A. Koseska *et al.*, J. Theor. Biol. **263,** 189 (2010).

[35] T. K. Berger, R. Perin, G. Silberberg, and H. Markram, J. Physiol. London **587,** 5411 (2009).

[36] M. S. Baptista and J. Kurths, Phys. Rev. E **77,** 026205 (2008).

Figure captions

Figure 1. Simulated coupling of droplets**. (a)** Curves 1-4 are from PDE simulations. curve 1: a = 0.01 cm, P_U= 1, $D_S = 10^{-5}$ cm^2 s^{-1}; curve 2: a = 0.01 cm, P_U = 0.01, $D_S = 10^{-5}$ cm^2 s^{-1}; curve 3: a = 0.003 cm, P_U = 0.01, $D_S = 10^{-5}$ cm^2 s^{-1}; curve 4: a = 0.003 cm, P_U = 0.01, $D_S = 10^{-6}$ cm^2 s^{-1}. Curve 5 is obtained from an ODE simulation at P_U = 0.01 and k_f = 0.3 s^{-1}. Time t_p = 1.7 s, $t_d = b^2/(2D_S)$ for PDEs and $t_d = P_U/(r_V k_f)$ for ODEs, since $t_d = k_b^{-1} = P_U/(r_V k_f)$. (**b**) Curves 1, 2, and 4 are from PDE (at $D_U = D_S = 10^{-5}$ cm^2 s^{-1}), curve 3 from ODEs. Curve 1: $a = 5 \times 10^{-4}$ cm, $b = 2 \times 10^{-3}$ cm; curve 2: $a = b = 2 \times 10^{-3}$ cm; curve 4: $a = 1 \times 10^{-2}$ cm, $b = 3 \times 10^{-4}$ cm; curve 3: k_f = 0.3 s^{-1}, r_V = 33 (= a/b for curve 4). (**c**) typical kinetics obtained from PDEs, $a = 1 \times 10^{-2}$ cm, $b = 3 \times 10^{-4}$ cm; P_U = 1, $u_1 = \int_0^a u dx/a$, $s = \int_a^{a+b} s dx/b$, $u_2 = \int_{a+b}^{2a+b} u dx/a$, $D_U = D_S = 10^{-5}$ cm^2 s^{-1}. (**d**) typical kinetics obtained from ODEs, k_f = 1, r_V = 10, P_U = 1. No flux boundary conditions are used for PDE simulations. u_{1_max} in panels (a) and (c) is 10^{-4}.

Figure 2. AP oscillations. Shape (a) is "normal", while shape (b) occurs close to the AP/T boundary. Parameters: k_f = 2 s^{-1}, r_V = 10, P_X = 0.003, [MA] = (a) 0.3 M, (b) 0.085 M.

Figure 3. Parametric plane k_f-P_X (a and b) showing three possible regimes (dynamical behavior) of two coupled BZ oscillators, IP, in-phase oscillations; AP, anti-phase oscillations; and T, Turing-like stationary pattern (= two different stable steady states) at [MA] = (a) 0.03 M and (b) 0.056 M. Panels (c) and (d) are the dependences of the regimes on P_X (c) and k_f (d) at constant k_f (= 1 s^{-1}) and P_X (= 0.0015), respectively, at [MA] = 0.03 M. In all cases, r_V = 10; P_U = 2.5. In panels (a) and (b), curve 1 marks the transition from AP to IP, curve 2 marks the

transition from T to IP, curve 3 is the transition from T to AP, curve 4 is for the transition from AP to IP, curve 6 is the transition from AP to T regime, if the parameter (k_f or P_X) is changed by small steps. Curve 5 is explained in the text.

Figure 4. Parametric plane k_f-[MA] (a) shows three different regimes of two coupled BZ oscillators: IP, AP, and T. Panels (b) and (c) are the dependences of the regimes on [MA] at constant $k_f = 2.3\ s^{-1}$ for (b) and $1.2\ s^{-1}$ for (c). Parameters: $P_X = 0.003$, $r_V = 10$; $P_U = 2.5$. Curves 1 – 6 in (a) have the same meaning as in Fig. 3. Note that on part of curve 3 (near the triple point, where the AP, IP, and T domains merge), the transitions from T to AP and *vice versa* occur at the same parameters without hysteresis. This transition is marked by a two-headed arrow.

Figure 5. Parametric planes [MA]-P_X at k_f = (a) $0.5\ s^{-1}$ and (b) $2\ s^{-1}$. The transition from T to AP (curve 3) is unidirectional at $k_f = 0.5\ s^{-1}$ and bidirectional (without hysteresis) at $k_f = 2\ s^{-1}$. Curve 1 (the transition from AP to IP) has a continuation in the T domain at $k_f = 0.5\ s^{-1}$. Curve 1′ in (a) is just a copy of curve 1 in (b) for easier comparison of the two parametric planes.

Figure 6. (a) r_V-P_X parametric plane divided by four straight lines obtained at different [MA]; **(b)** C_U-C_X parametric plane; since $C_U < k_f$ and $k_f = 1\ s^{-1}$, C_U cannot be larger than $1\ s^{-1}$ in this case. (c) and (d) kinetic curves at different [MA]. Parameters: $k_9' = 0.12\ M^{-1}s^{-1}$, (**a**) $k_f = 0.3\ s^{-1}$, [MA]/M = (1) 0.5, (2) 0.2, (3) 0.08, (4) 0.02; (**b**) $k_f = 1\ s^{-1}$, [MA] = 0.1 M, r_V and P_X are varied; (**c**), (**d**) [MA]/M = (1) 1.5, (2) 0.6, (3) 0.3, (4) 0.1, (5) 0.04. Time $t = 7$ s in (c) and (d) corresponds to the maximum of the activator concentration (peak of the autocatalysis).

Figure 7. Trajectory of the triple point in the 3D space k_f-P_X - [MA] presented as two projections on the k_f-P_X and k_f -[MA] planes: curves "P_X" and "MA", respectively. Parameters: $r_V = 10$, $P_U = 2.5$. Dotted line in (b) is a segment of "P_X" in (a). Curves 1a and 1b in (b) correspond to curves 1 in Figs. 3(a) and 3(b), respectively.

Figure 8. (Color online) (a)-(c). Space-time plots for 3 circularly coupled droplets. (a) Turing pattern, (b) Anti-phase oscillatory clusters (APOC), (c) In-phase oscillations (IP). Global period T_g/s = (b) 1421, (c) 1143. T-patterns is observed at P_X = 0-0.02, APOC at P_X = 0.0035-0.004, IP exist at any P_X. (d)-(g). Patterns for 4 circularly coupled droplets. (d) T, (e) AP, (f) APOC, (g) Anti-phase oscillatory clusters with common droplet (APOCwCD); IP oscillations are not shown for 4 droplets, since they are the same with the same period, 1143 s, for any number of droplets. Global period T_g/s = (e) 1446, (f) 1398, (g) 1560. T-pattern is observed at P_X = 0-0.0045, AP at 0-0.003, APOC at 0.001-0.005, and APOCwCD at 0.005-0.006. Parameters: [MA] = 0.02 M, k_f = 0.45 s^{-1}, h = 0.15 M, [A] = 0.3 M, P_U = 2.5, r_V = 10.

Figure 9. (Color online) Patterns for 5 circularly coupled droplets. (a) T, (b) Two anti-phase oscillatory clusters with special droplet [2APOC(1:2)wSD], (c) APOC, patterns (d) and (e) can be interpreted (although not precisely) as mixtures of APOC and APOCwCD patterns. Global period T_g/s = (b) 3367, (c) 1331, (d) 4175, (e) 2842. T-pattern is observed at P_X = 0-0.015, pattern (b) at 0.001-0.002, (c) 0.003-0.004, (d) 0.005, (e) 0.006-0.007. At $P_X > 0.008$, only IP oscillations exist.

Figure 10. (Color online) Patterns for 6 circularly coupled droplets. T-pattern in (a) is observed at P_X = 0-0.02, (b) AP at 0 - 0.003, (c) APOC at 0.002-0.007, and (d) 2APOC(1:2)wSD at 0.0025-0.0035. At $P_X > 0.008$, only IP oscillations exist. Global period T_g/s = (b) 1451, (c) 1285, (d) 2596.

Figure 11. (Color online) Patterns for 7 circularly coupled droplets. Pattern (a) is observed at P_X = 0.003, (b) at P_X = 0-0.0026, (c) 2APOC(1:2)wSD at 0.0028-0.0033, (d) 0.003-0.007. At $P_X > 0.008$, only IP oscillations exist. Global period T_g/s = (a) 1164, (c) 2487, (d) 1260. Parameters: [MA] = 0.02 M, k_f/s^{-1}= (a) 0.3, (b)-(d 0.45, h = 0.15 M, [A] = 0.3 M, P_U = 2.5, r_V = 10. Turing pattern at small P_X is stable at $k_f > 0.4$, while AP patterns [like (a) at $k_f = 0.3\ s^{-1}$] are more stable at smaller k_f. Due to odd number of droplets and periodic boundary conditions, two droplets in (a) oscillate in-phase.

Figure 12. (Color online) Patterns for 8 circularly coupled droplets [except (j), where 6 droplets and $u_T = x_T = 0$ boundary condition]. Patterns are observed at P_X = (a) (T-pattern) 0 - 0.008, another Turing pattern (not shown) with droplets 1 and 4 in the oxidized state and all others in the reduced state is stable at P_X = 0 - 0.0035, (b) (AP) 0 - 0.003, (c) (moving defect) 0.0033-0.004, (d) (moving defect) and (e) (APOC) 0.005, (f) (APOCwCD) 0.01. Global period T_g/s = (b) 1452, (c) 3753, (d) 9210, (e) 1230, (f) 1300. Parameters: [MA] = 0.02 M, $k_f = 0.45\ s^{-1}$, h = 0.15 M, A = 0.3 M, P_U = 2.5, r_V = 10. Parameters for moving defect (g): 6 droplets, $u_T = x_T = 0$, [MA] = 0.06, $k_f = 0.138\ s^{-1}$, P_X = 0.1, h = 0.08 M, A = 0.3 M.

Figure 13. (Color online) Patterns for 9 circularly coupled droplets. (a) T-pattern, (b) and (c) Three anti-phase oscillatory clusters with special droplet [3APOC(1:2:2)wSD], (d) similar to AOCwCD but one cluster consisting of droplets 1, 4-6, and 9 oscillates temporally and periodically with a small phase shift between droplets 1, 9 and droplets 4-6; (e) APOC, (f) similar to APOCwCD, but with two common droplets and one defect. Pattern (a) is observed at $P_X = 0.02$, (b) at 0.002 – 0.003, (c) 0.0035, (d) and (e) 0.005, (f) 0.01. Global period T_g/s = (b) 2870, (c) 4260, (d) 2861, (e) 1214, (f) 8943. Parameters as in Fig. 8.

Figure 14. (Color online) Effect of boundary conditions on space-time plots for 5 droplets. (a) Periodic boundary conditions; (b) $u_T = 4 \times 10^{-6}$ M, $x_T = 6 \times 10^{-8}$ M; (c) $u_T = x_T = 0$. Parameters: [MA] = 0.03 M, $k_f = 0.3$, $P_X = 0.001$. $h = 0.15$ M, [A] = 0.3 M, $P_U = 2.5$, $r_V = 10$. (a) Cascade patterns (similar to AP), (b) Turing (drops 1, 2, and 5) plus AP, (c) T-patterns.

Figure 15. (Color online) Space-time plots for 5 droplets coupled in-line with boundary conditions $u_T = 4 \times 10^{-6}$ M and $x_T = 6 \times 10^{-8}$ M for increasing P_X = (a) 0.001-0.002, (b) and (c) 0.005, (d) and (e) 0.01, (f) 0.03. Parameters: [MA] = 0.04 M, $k_f = 0.3$ s^{-1}, $h = 0.15$ M, [A] = 0.3 M, $P_U = 2.5$, $r_V = 10$.

Figure 16. (Color online) Space-time plots for 6 droplets coupled in-line with boundary conditions $u_T = x_T = 0$ for increasing k_f. k_f/s^{-1}= (a) 0.2, (b) 0.2-0.4, (c) 0.2, (d) 0.3, (e) 0.4, (f) 0.5. Parameters: [MA] = 0.035 M, $P_X = 0.004$; $h = 0.15$ M, $A = 0.3$ M, $P_U = 2.5$, $r_V = 10$.

Figure 17. (Color online) Space-time plots for 5 droplets coupled in-line with boundary conditions $u_T = 4 \times 10^{-6}$ M and $x_T = 7 \times 10^{-8}$ M for increasing k_f. k_f/s^{-1}= (a) 0.1, (b) 0.15, (c) 0.2, (d) 0.25-0.3, (e) 0.4. Parameters: [MA] = 0.03 M, $P_X = 0.015$; $h = 0.15$ M, $A = 0.3$ M, $P_U = 2.5$, $r_V = 10$.

Figure 18. (Color online) Space-time plots for 5 droplets coupled in-line with boundary conditions $u_T = 4 \times 10^{-6}$ M and $x_T = 7 \times 10^{-8}$ M for increasing [MA]. [MA]/M = (a) 0.02-0.025, (b) 0.03-0.035, (c) 0.05, (d) 0.1, (e) 0.2-0.8. Parameters: $k_f = 0.3$ s^{-1}, $P_X = 0.015$.

Figure 19. Scheme for two coupled droplets

Figures

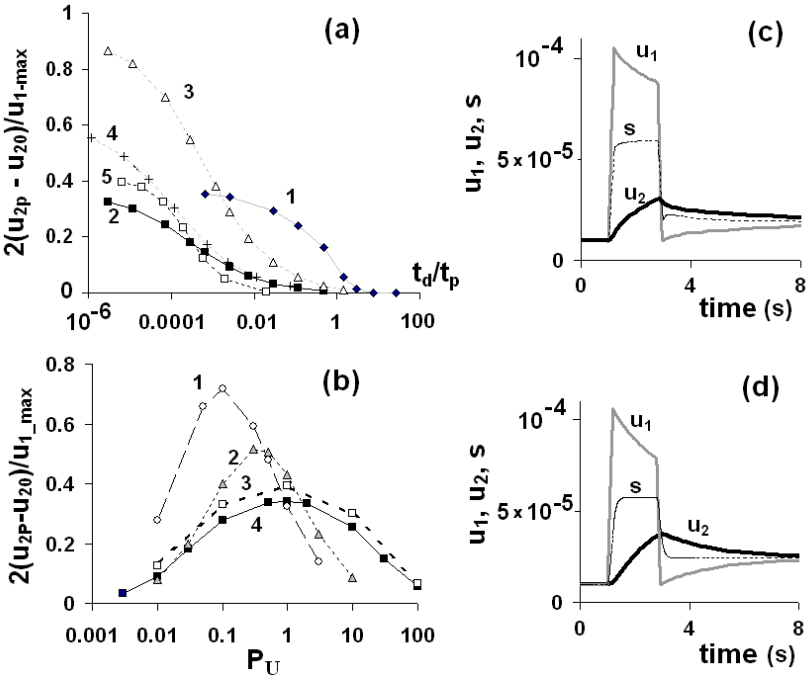

Figure 1

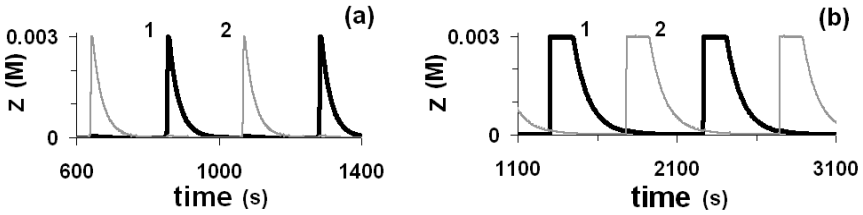
(a)
1
2
0.003
z (M)
0
600
1000
1400
time (s)
(b)
1
2
0.003
z (M)
0
1100
2100
3100
time (s)

Figure 2

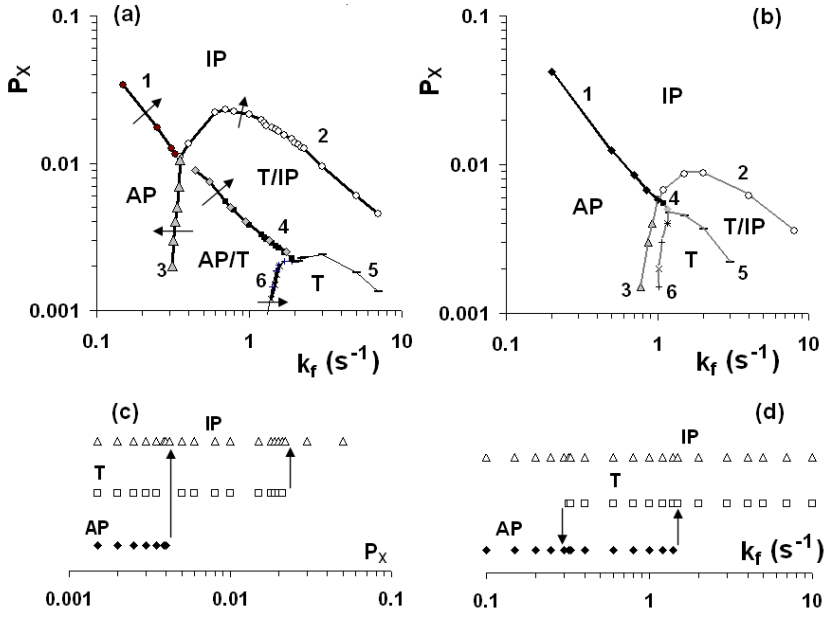

Figure 3

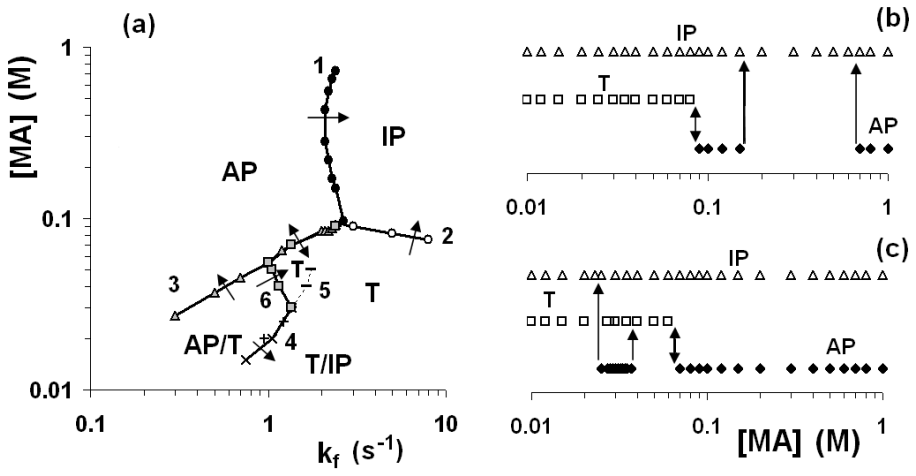
(a)
[MA] (M)
1
0.1
0.01
0.1
1
10
k_f (s^{-1})
IP
AP
T
AP/T
T/IP
1
2
3
4
5
6
(b)
IP
T
AP
0.01
0.1
1
(c)
IP
T
AP
0.01
0.1
1
[MA] (M)

Figure 4

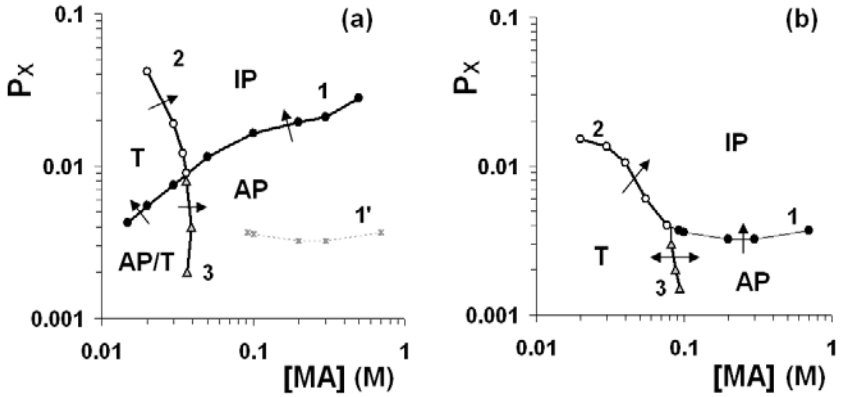

Figure 5

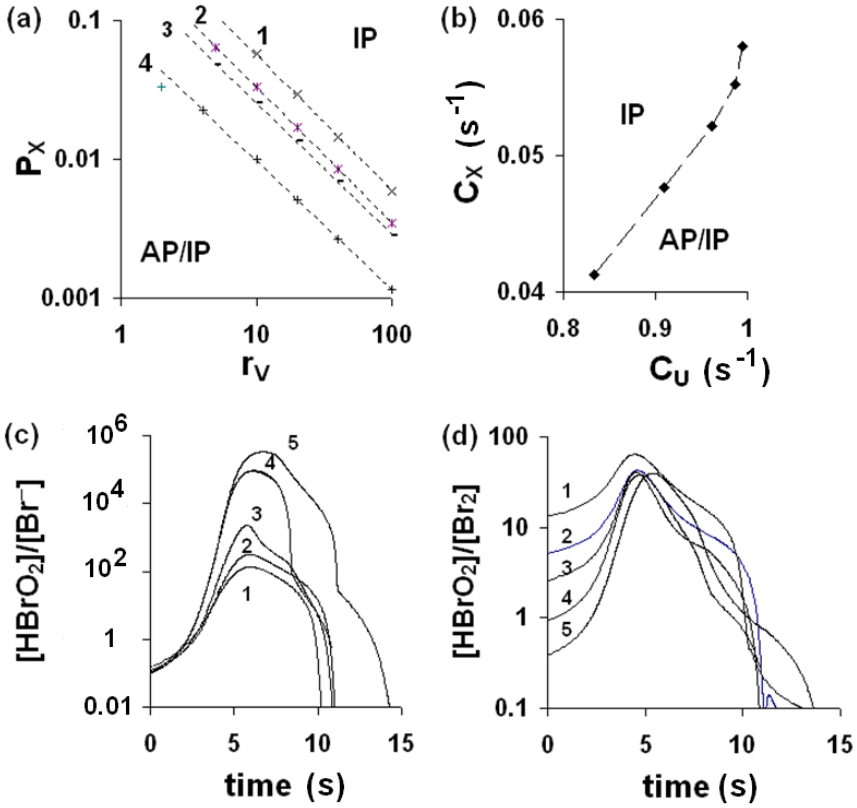
(a)
0.1
0.01
0.001
P_X
1
10
100
r_V
IP
AP/IP
1
2
3
4
(b)
0.06
0.05
0.04
C_X (s^{-1})
0.8
0.9
1
C_U (s^{-1})
IP
AP/IP
(c)
10^6
10^4
10^2
1
0.01
$[HBrO_2]/[Br^-]$
0
5
10
15
time (s)
1
2
3
4
5
(d)
100
10
1
0.1
$[HBrO_2]/[Br_2]$
0
5
10
15
time (s)
1
2
3
4
5

Figure 6

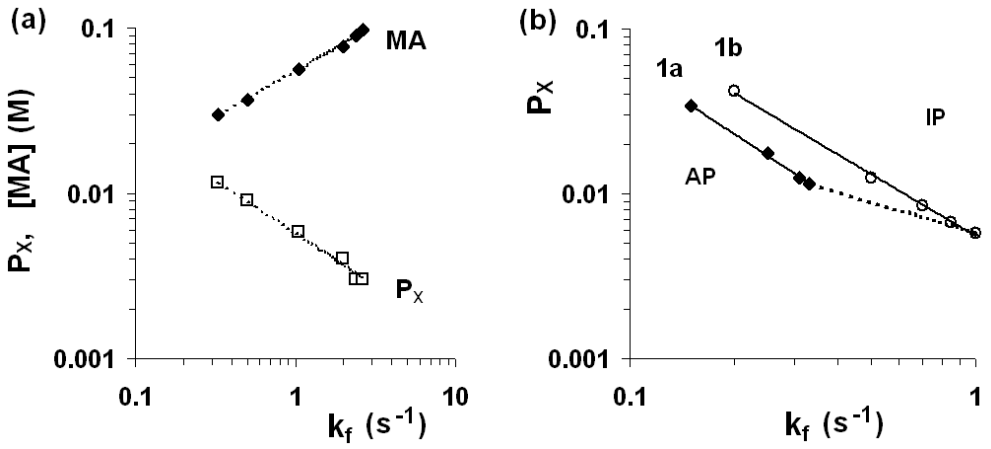
(a)
0.1
0.01
0.001
P_X, [MA] (M)
MA
P_X
0.1
1
10
k_f (s^{-1})
(b)
0.1
0.01
0.001
P_X
1a
1b
IP
AP
0.1
1
k_f (s^{-1})

Figure 7.

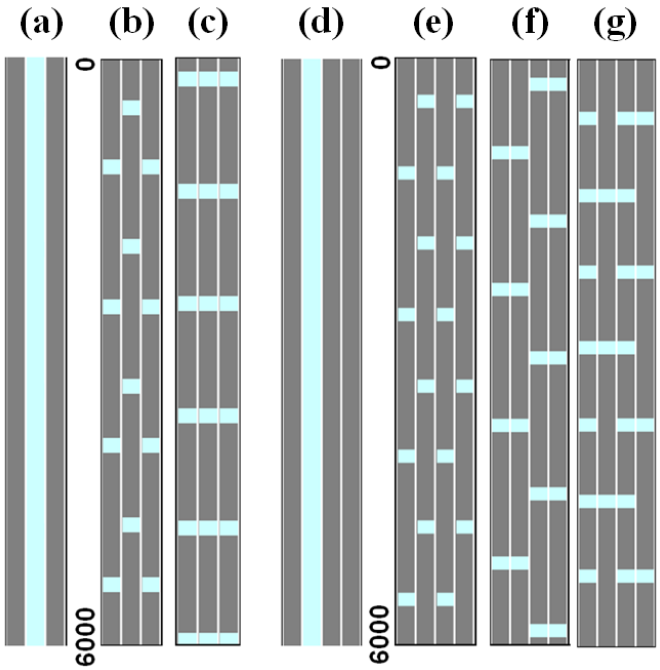

Figure 8.

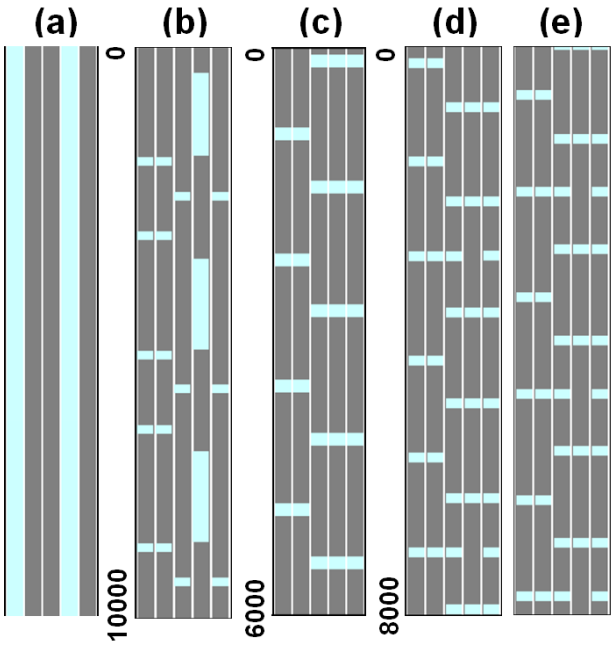

Figure 9.

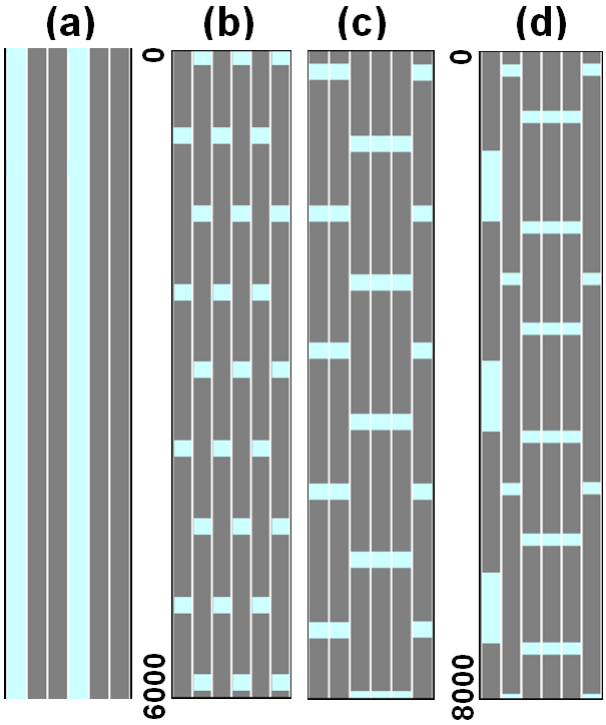

Figure 10.

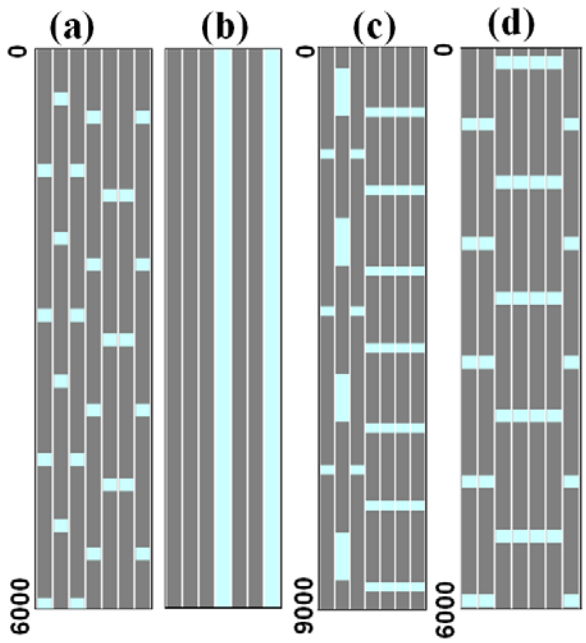

Figure 11.

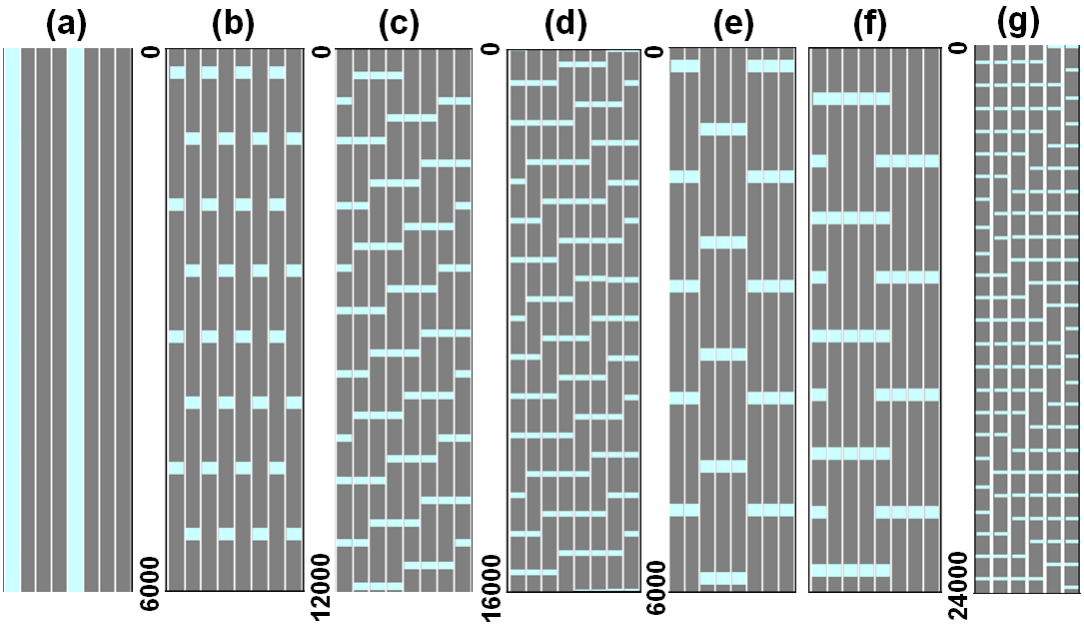

Figure 12.

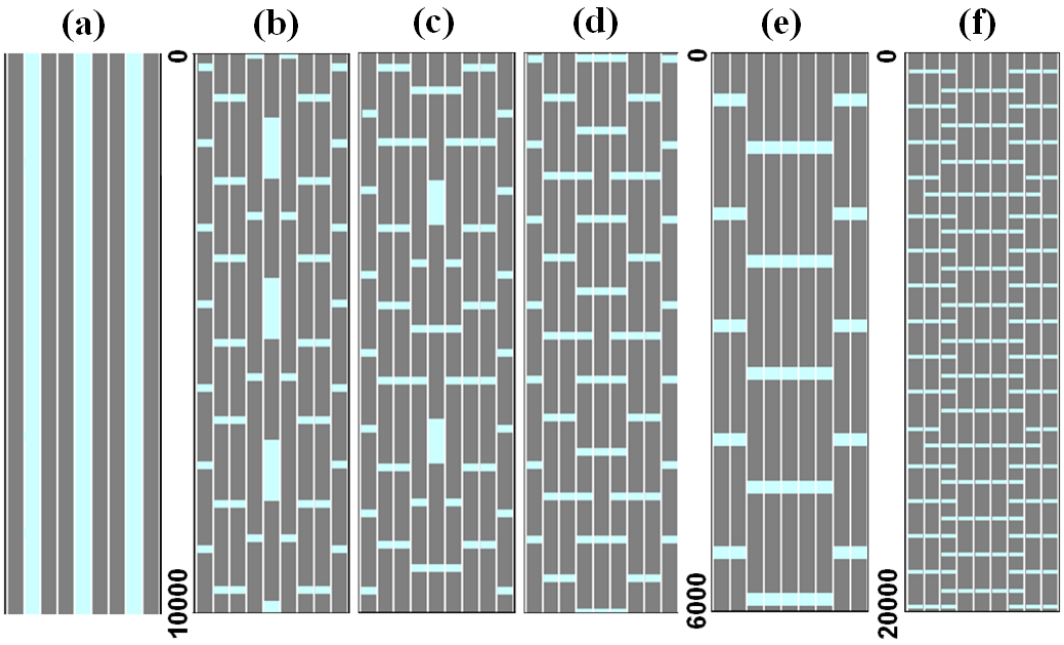

Figure 13.

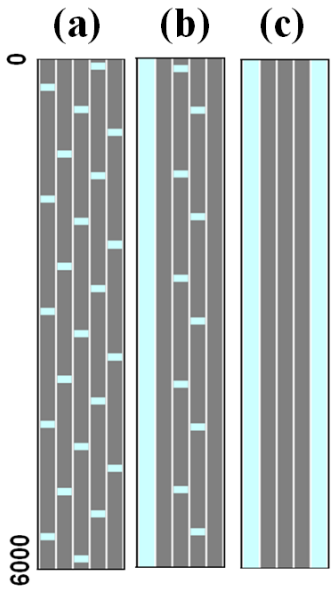

Figure 14.

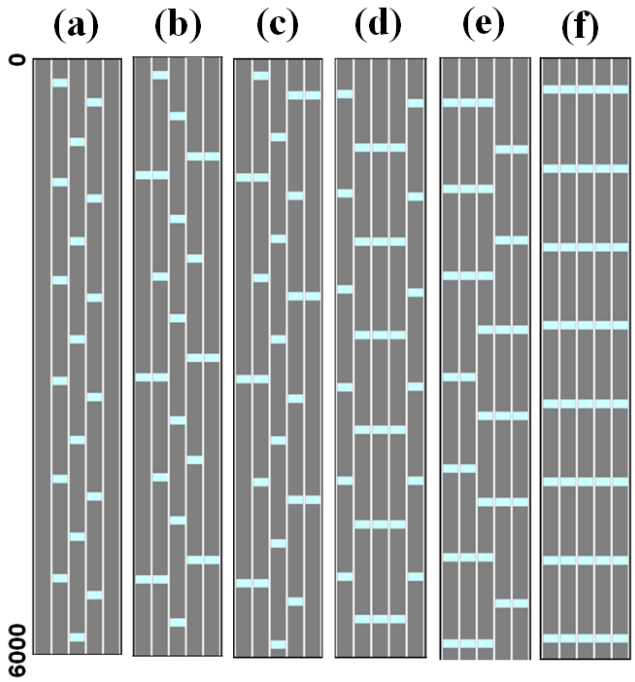

Figure 15.

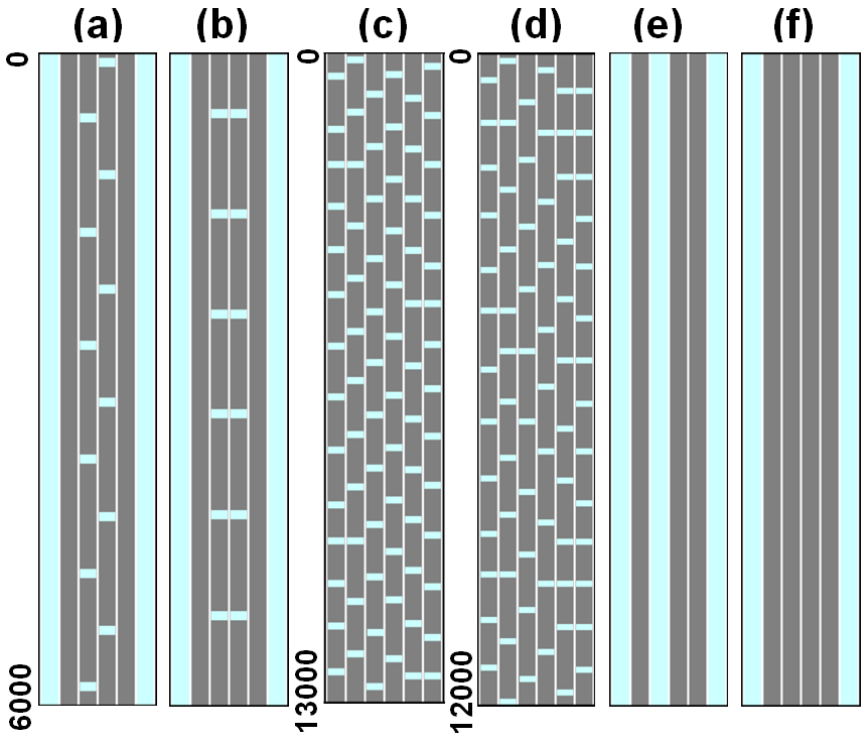

Figure 16.

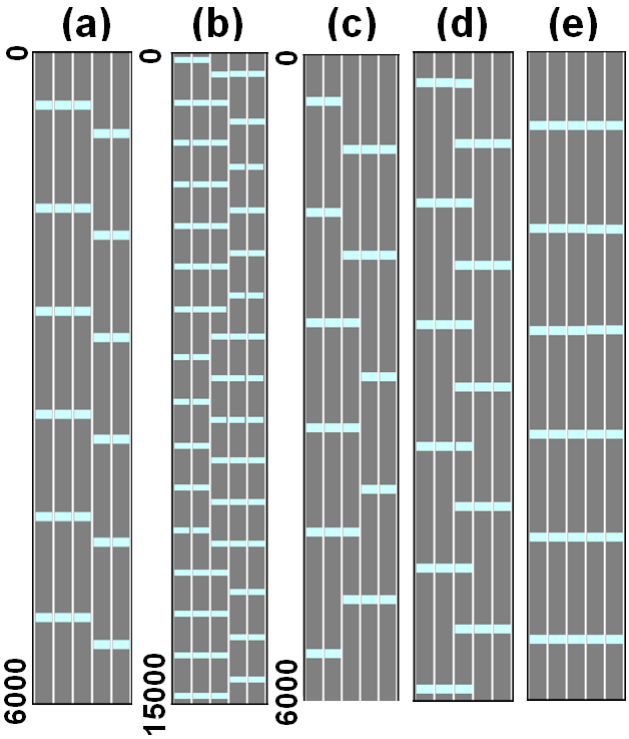

Figure 17.

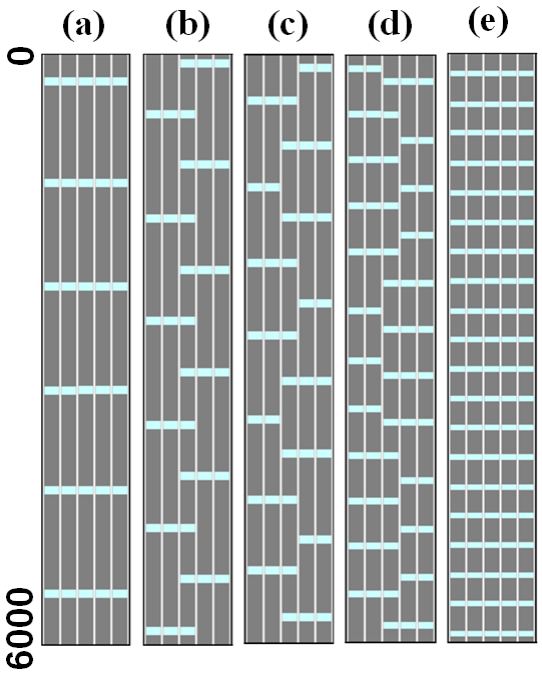

Figure 18.

Appendix 1. Mass exchange between two water droplets with length *a* and oil gap *b* is simulated by PDEs that describe the scheme shown in Figure 19.

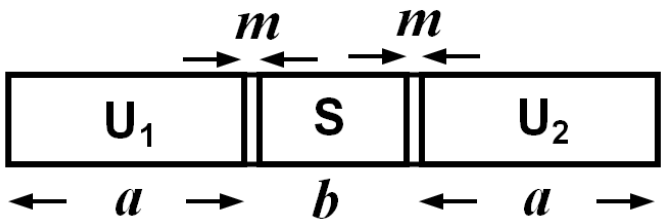

Fig. 19

The passage of molecules through a liquid/liquid interface can be envisioned with the aid of a very thin (a few molecules wide) layer (boundary regions "*m*" with length *m*), where diffusion of both molecules U_1 (U_2) and S is allowed. In these regions, we introduce equilibrium reactions: $U_1 \leftrightarrow S$ for the left boundary region "*m*" and $U_2 \leftrightarrow S$ for the right boundary region "*m*". The rate constant for reaction $U_1 \rightarrow S$ is $k_{US1} = 4000\ s^{-1}$, which is chosen arbitrarily large. The rate constant for back reaction $S \rightarrow U_1$ is $k_{SU1} = k_{US1}/P_U$, where P_U is the partition coefficient. Similar expressions hold for the rate constants in the right boundary region "*m*" (constants $k_{US2} = k_{US1}$ and $k_{SU2} = k_{SU1}$). If length *m* is chosen very small (10^{-10} -10^{-9} nm), then the computation time becomes extremely long. To overcome this technical problem, we increase *m* to 10^{-6} - 10^{-5} cm depending on the sizes *a* and *b*, which are kept two to three orders of magnitude larger than *m*. The constant k_{US1} is chosen so large and the length *m* so small that their values have no effect on the dynamics of mass exchange. The constants k_{US2}, k_{US1}, k_{SU2}, and k_{SU1} are zero outside the regions "*m*". Molecules S (U) cannot diffuse in regions "*a*" ("*b*"), but can diffuse in regions "*m*". The PDEs then take the form

$$\partial[U_1]/dt = - k_{US1}[U_1] + k_{SU1}[S] + P_1 + D_U\partial^2[U_1]/d\xi^2 \quad (A1)$$

$$\partial[S]/dt = k_{US1}[U_1] + k_{US2}[U_2] - (k_{SU1} + k_{SU2})[S] + D_S\partial^2[S]/d\xi^2 \quad (A2)$$

$$\partial[U_2]/dt = - k_{US2}[U_2] + k_{SU2}[S] + D_U\partial^2[U_2]/d\xi^2 \quad (A3)$$

where the perturbation P_1 is composed of two pulses with "positive" amplitude A_1 and "negative" amplitude A_2 and is written as

$$P_1 = [A_1 \times \mathrm{UPULSE}(t - t_1, t - t_2) - A_2 \times \mathrm{UPULSE}(t - t_3, t - t_4) \times \mathrm{USTEP}([\mathrm{U}_1] - [\mathrm{U}_1]_0)] \times \mathrm{USTEP}(a - \xi) \quad \text{(A4)}$$

where $A_1 = A_2 = 5 \times 10^{-4}$, $\Delta t = t_2 - t_1 = t_4 - t_3 = 0.2$ s, $t_1 = 1$ s, $t_3 = 2.8$ s. The function USTEP(*arg*) is equal to 1 if the argument *arg* is positive and 0 if the argument is negative, the function UPULSE(arg_1, arg_2) is equal to 1 if arg_1 is positive and arg_2 is negative and 0 everywhere else. At $A_1 = 5 \times 10^{-4}$ and $t_2 - t_1 = 0.2$, the maximum value of $[\mathrm{U}_1]$ reaches approximately 10^{-4} (at $t = t_2$), which is our value of u_{1_max} used for calculating the response $R = 2(u_{2p} - u_{20})/u_{1\_max}$, where u_{2p} is the value of $u_2 = \int_{a+b}^{2a+b} [\mathrm{U}_2] d\xi / a$ taken at the end of the "negative" pulse (with amplitude A_2) at $t = t_4 = 3$ s (u_2 reaches its maximum value at that time in Fig. 1c and 1d). Initial conditions: $[\mathrm{U}_1] = [\mathrm{U}_1]_0 \times \mathrm{USTEP}(a - \xi)$, $[\mathrm{S}] = [\mathrm{S}]_0 \times \mathrm{UPULSE}(\xi - a - m, \xi - a - b - m)$, $[\mathrm{U}_2] = [\mathrm{U}_2]_0 \times \mathrm{USTEP}(\xi - a - b - 2m)$, $[\mathrm{U}_1]_0 = [\mathrm{U}_2]_0 = 10^{-5}$, $[\mathrm{S}]_0 = [\mathrm{U}_1]_0 P_U$.